Numerical and experimental time-domain characterization of terahertz conducting polymers

Article (Accepted Version)

Numerical and Experimental Time-Domain Characterization of Terahertz Conducting Polymers

Dimitrios C. Zografopoulos, Konstantinos P. Prokopidis, Antonio Ferraro, Luke Peters, Marco Peccianti, and Romeo Beccherelli

***Abstract*—A comprehensive framework for the theoretical and experimental investigation of thin conducting films for terahertz applications is presented. The electromagnetic properties of conducting polymers spin-coated on low-loss dielectric substrates are characterized by means of terahertz time-domain spectroscopy and interpreted through the Drude-Smith model. The analysis is complemented by an advanced finite-difference time-domain algorithm, which rigorously deals both with the dispersive nature of the involved materials and the extremely subwavelength thickness of the conducting films. Significant agreement is observed among experimental measurements, numerical simulations, and theoretical results. The proposed approach provides a complete toolbox for the engineering of terahertz optoelectronic devices.**

***Index Terms*—Transparent electrodes, terahertz science, finite-different time-domain method, time-domain spectroscopy.**

I. Introduction

Rapid advances are observed in the field of terahertz (THz) technology and its applications in fields such as spectroscopy, wireless communications, and bioimaging [1]. Much of this progress relies on the development of functional materials, e.g. thin conducting films (TCF) that serve the key role of transparent electrodes for the application of control electric signals in THz optoelectronic devices [2], [3]. A primary, but not sole, candidate for this scope is poly(3,4-ethylenedioxythiophene) poly(styrenesulfonate) (PEDOT:PSS) [4].

The performance of TCF is determined mainly by their conductivity and transparency, which in turn depend on the film thickness, the substrate, and the device layout. Hence, the theoretical and experimental characterization of TCF electromagnetic (EM) properties is indispensable for the engineering of THz optoelectronic devices. Compared to bulky conducting materials, such as metals, whose EM response follows the Drude model (electron gas), carriers in TCF can be localized and trapped leading to back-scattering events. This behavior can be captured by an extended Drude-Smith (DS) model [5], which has provided excellent fits for numerous TFC, among which Ag nanowires [6], PEDOT:PSS [4], [7], ZnO films and nanowires [8], [9], ITO nanowhiskers [10], phase transitions in vanadium oxide films [11], and silicon nanocrystals [12].

One of the most popular THz characterization techniques, also routinely employed to investigate TCF, is time-domain spectroscopy (THz-TDS), where the material under test (MUT) is probed with picosecond pulses of THz radiation. The MUT properties are deduced by processing the information on the amplitude and the phase of the transmitted wave [13]. The numerical counterpart of the THz-TDS experimental studies is the finite-difference time-domain (FDTD) method [14], [15], a powerful tool for the time-domain studies of complex EM structures. However, the direct implementation of FDTD in the study of THz-TCF is hindered by two issues: i) the incorporation of the DS dispersive model and ii) the treatment of extremely sub-wavelength TCF thicknesses, typically more than three orders of magnitude smaller than the THz wavelength. The latter, in particular, imposes unnecessarily small temporal steps, by virtue of the Courant-Friedrichs-Lewy condition, which lead to very long computational times in the case of standard FDTD formulations [14].

In this work we provide a framework for the study of THz-TCF, tested on commercially available PEDOT:PSS polymers characterized via THz-TDS. The experimentally measured properties are fitted to the DS model, yielding results consistent with the polymer nominal properties. The investigation is backed by a subcell FDTD formulation that tackles both the dispersive nature and arbitrary TCF thicknesses, being more robust than its conventional uniform-grid counterpart. Although subcell FDTD techniques for thin films are known [16], [17], the proposed algorithm enables the modelling of DS-TCF placed between a Debye medium and a plain dielectric. Hence, it addresses the relevant paradigm for the study of THz-TCF, without being restricted to the specific choice of materials and frequencies. Very good agreement is observed between theoretical, numerical, and experimental results, highlighting the validity of the proposed approach.

II. Theoretical and Experimental Studies of Terahertz Thin Conducting Films

The sample geometry and the THz-TDS setup for its characterization are shown in Fig. 1(a,b). A thin layer of PEDOT:PSS is spin-coated on a dielectric substrate, the thicknesses of the two layers being t and h, respectively. Figure 1(c) shows the FDTD Yee cell of the employed subcell modelling technique that encompasses the TCF ($\delta_2 \equiv t$). The total cell thickness is $\Delta z = \delta_1 + \delta_2 + \delta_3$, with Δz being the FDTD spatial discretization step. The TCF medium #2 lies between two

D. C. Zografopoulos, A. Ferraro, and R. Beccherelli are with the Consiglio Nazionale delle Ricerche, Istituto per la Microelettronica e Microsistemi (CNR-IMM), Rome 00133, Italy (e-mail: dimitrios.zografopoulos@artov.imm.cnr.it).

K. P. Prokopidis is with the Department of Electrical and Computer Engineering, Aristotle University of Thessaloniki, Thessaloniki 54124, Greece.

L. Peters and M. Peccianti are with the Emergent Photonics Lab (EPic), Department of Physics and Astronomy, University of Sussex, Falmer, Brighton BN1 9RH, UK.

MP acknowledges support from the European Union's Horizon 2020 research and innovation programme, grant agreement no. 725046.

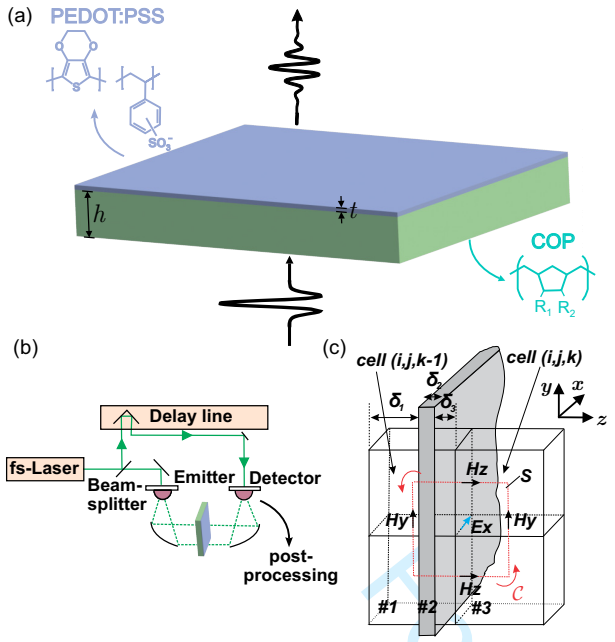

Fig. 1. (a) Layout of the investigated sample, (b) description of the THz-TDS measurement setup, and (c) Yee cell of the proposed subcell FDTD algorithm.

dielectric media #1 and #3 with an overall thickness larger than Δz, and it is positioned such that $\delta_2 \leq \Delta z/2$ and $\delta_3 \leq \Delta z/2$.

Assuming an $e^{j\omega t}$ time dependence, the TCF relative permittivity is described by the DS model defined as [4], [5]

$$\varepsilon_{DS}(\omega) = \varepsilon_{DS,\infty} + \frac{\omega_p^2}{j\omega(\gamma + j\omega)}\left(1 + \frac{c\gamma}{\gamma + j\omega}\right) \quad (1)$$

$$= \varepsilon_{DS,\infty} + \frac{\omega_p^2}{j\omega(\gamma + j\omega)} + \frac{\omega_p^2 c\gamma}{j\omega(\gamma + j\omega)^2}$$

$$= \varepsilon_{DS,\infty} + \chi_{DS1}(\omega) + \chi_{DS2}(\omega), \quad (2)$$

where ω_p is the electron plasma frequency, γ is the damping rate, c is the fraction of the initial velocity of carriers ($-1 \leq c \leq 0$) and $\varepsilon_{DS,\infty}$ is the relative permittivity at infinite frequency. The term χ_{DS1} is the standard Drude expression of the electric susceptibility, while χ_{DS2} is a third-order term with respect to the angular frequency ω, corresponding to the extension proposed by Smith [5].

Medium #1 is considered to be a dielectric substrate with Debye relative permittivity given by

$$\varepsilon_D(\omega) = \varepsilon_{D,\infty} + \frac{\varepsilon_{D,s} - \varepsilon_{D,\infty}}{1 + j\omega\tau} = \varepsilon_{D,\infty} + \chi_D(\omega), \quad (3)$$

where $\varepsilon_{D,\infty}$ and $\varepsilon_{D,s}$ are the relative permittivities at the high and low frequency limit, respectively, and τ is the characteristic relaxation time of the medium. This selection significantly broadens the applicability of the algorithm, as many dielectric substrates in the microwave and THz spectrum are well approximated as Debye media. Last, medium #3 is a non-dispersive dielectric.

Here, we briefly provide the salient points for the derivation of the proposed FDTD formulation. Ampère-Maxwell's equation in the integral form reads

$$\iint_S \frac{\partial \boldsymbol{D}}{\partial t} d\boldsymbol{S} = \oint_C \boldsymbol{H} d\boldsymbol{l} \quad (4)$$

where the contour C and the surface S are shown in the Fig. 1(c). The contour integral I_c at time step $n + 1/2$ is

$$I_c^{n+\frac{1}{2}} = \oint_C \boldsymbol{H}^{n+\frac{1}{2}} d\boldsymbol{l}$$

$$= H_y^{n+\frac{1}{2}}(i+\tfrac{1}{2}, j, k+\tfrac{1}{2})\Delta y - H_z^{n+\frac{1}{2}}(i+\tfrac{1}{2}, j+\tfrac{1}{2}, k)\Delta z$$

$$- H_y^{n+\frac{1}{2}}(i+\tfrac{1}{2}, j, k-\frac{1}{2})\Delta y + H_z^{n+\frac{1}{2}}(i+\tfrac{1}{2}, j-\tfrac{1}{2}, k)\Delta z \quad (5)$$

where Δy is the cell size in y-direction. The left-hand side of (4) is discretized using central differences

$$D_{tx}^{n+1}(i+\tfrac{1}{2}, j, k) = D_{tx}^{n}(i+\tfrac{1}{2}, j, k) - \frac{\Delta t}{\Delta y \Delta z} I_c^{n+\frac{1}{2}} \quad (6)$$

where D_{tx} is the total dielectric displacement perpendicular to the surface S and Δt is the time step of the FDTD algorithm. D_{tx} is defined as the sum of its x-components in the three media, weighted by the partial surfaces s_1, s_2 and s_3, i.e., $D_{tx} = s_1 D_{1x} + s_2 D_{2x} + s_3 D_{3x}$, where

$$s_1 = \frac{1}{2} - \frac{\delta_2 + \delta_3}{\Delta z}, s_2 = \frac{\delta_2}{\Delta z}, s_3 = \frac{1}{2} + \frac{\delta_3}{\Delta z}. \quad (7)$$

For the three media here considered (Debye, DS, and plain dielectric) the total $D_t(\omega)$ is given by

$$D_t(\omega) = \varepsilon_0 \left(s_1 \varepsilon_D(\omega) E_1(\omega) + s_2 \varepsilon_{DS}(\omega) E_2(\omega) + s_3 \varepsilon_3 E_3(\omega)\right), \quad (8)$$

where we dropped the subscript x for brevity and ε_0 is the vacuum permittivity. The application of the boundary conditions between the adjacent materials yields $E_1 = E_2 = E_3 = E$. After the substitution of the relative permittivities of (3) and (2) in (8) we get

$$D_t(\omega) = \varepsilon_0(\varepsilon_{\infty,\text{eff}} E(\omega) + s_1 F_D(\omega) + s_2 F_1(\omega) + s_2 F_2(\omega)), \quad (9)$$

where $\varepsilon_{\infty,\text{eff}} = s_1 \varepsilon_{D,\infty} + s_2 \varepsilon_{DS,\infty} + s_3 \varepsilon_3$ and the terms F_D, F_1, and F_2 are given by

$$F_D(\omega) = \chi_D(\omega) E(\omega), \; F_1(\omega) = \chi_{DS1}(\omega) E(\omega), \; F_2(\omega) = \chi_{DS2}(\omega) E(\omega). \quad (10)$$

Equation (9) is transformed into the time domain

$$D_t^{n+1} = \varepsilon_0(\varepsilon_{\infty,\text{eff}} E^{n+1} + s_1 F_D^{n+1} + s_2 F_1^{n+1} + s_2 F_2^{n+1}). \quad (11)$$

We then apply to (10) the bilinear z-transform, a conformal mapping technique from ω-plane to z-plane commonly used in digital processing techniques,

$$j\omega = \frac{2}{\Delta t} \frac{1 - z^{-1}}{1 + z^{-1}} \quad (12)$$

thus obtaining

$$F_D(z) = \chi_D(z) E(z), \; F_1(z) = \chi_{DS1}(z) E(z), \; F_2(z) = \chi_{DS2}(z) E(z), \quad (13)$$

with $\chi_D(z)$, $\chi_{DS1}(z)$, $\chi_{DS2}(z)$ described by

$$\chi_D(z) = \frac{a_0 + a_1 z^{-1}}{b_0 + b_1 z^{-1}}, \chi_{DS1}(z) = \frac{c_0 + c_1 z^{-1} + c_2 z^{-2}}{d_0 + d_1 z^{-1} + d_2 z^{-2}}$$

$$\chi_{DS2}(z) = \frac{e_0 + e_1 z^{-1} + e_2 z^{-2} + e_3 z^{-3}}{f_0 + f_1 z^{-1} + f_2 z^{-2} + f_3 z^{-3}}, \quad (14)$$

TABLE I
FITTED DS PARAMETERS FOR EXPERIMENTALLY INVESTIGATED PEDOT:PSS SAMPLES.

Material	$\varepsilon_{DS,\infty}$	$\omega_p/2\pi$ [THz]	$\gamma/2\pi$ [THz]	c	$\sigma_{0,\mathrm{DS}}$ [S/cm]	σ_0 [S/cm]
Orgacon HIL-1005[7]	470	53	2.2	−0.23	547	540
Clevios P Jet 700	293	54.59	1.4	−0.44	663	667

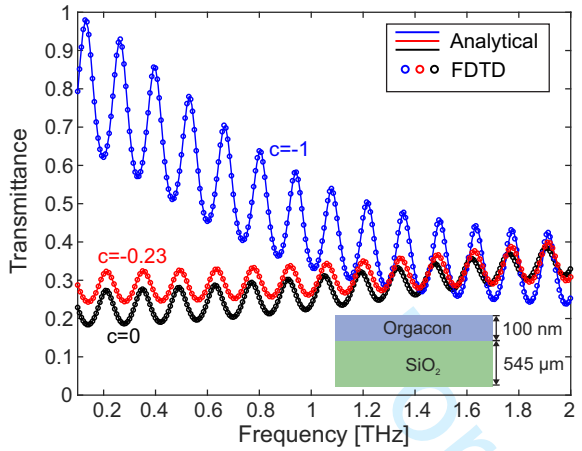

Fig. 2. Transmittance of a 100-nm PEDOT:PSS (Orgacon HIL-1005) layer on top of a SiO_2 substrate calculated by the proposed FDTD method. The limiting cases of the Smith extension (Drude model and full backscattering) are also included. Excellent agreement with the analytical solution is observed.

where

$$a_0 = a_1 = (\varepsilon_{D,s} - \varepsilon_{D,\infty})\Delta t \tag{15a}$$
$$b_0 = \Delta t + 2\tau, b_1 = \Delta t - 2\tau \tag{15b}$$
$$c_0 = c_2 = \omega_p^2 \Delta t^2,\ c_1 = 2c_0, \tag{15c}$$
$$d_0 = 4 + 2\gamma\Delta t,\ d_1 = -8,\ d_2 = 4 - 2\gamma\Delta t \tag{15d}$$
$$e_0 = \omega_p^2 c\gamma\Delta t^3,\ e_1 = 3e_0,\ e_2 = 3e_0,\ e_3 = e_0 \tag{15e}$$
$$f_0 = 8 + 8\gamma\Delta t + 2\gamma^2\Delta t^2, \tag{15f}$$
$$f_1 = -24 - 8\gamma\Delta t + 2\gamma^2\Delta t^2, \tag{15g}$$
$$f_2 = 24 - 8\gamma\Delta t - 2\gamma^2\Delta t^2, \tag{15h}$$
$$f_3 = -8 + 8\gamma\Delta t - 2\gamma^2\Delta t^2 \tag{15i}$$

By transforming (13) into the time domain we obtain the update equations for F_D, F_1 and F_2 through

$$F_D^{n+1} = \frac{a_0}{b_0}E^{n+1} + \frac{a_1}{b_0}E^n - \frac{b_1}{b_0}F_D^n, \tag{16a}$$
$$F_1^{n+1} = \sum_{m=0}^{2}\frac{c_m}{d_0}E^{n+1-m} - \sum_{m=1}^{2}\frac{d_m}{d_0}F_1^{n+1-m}, \tag{16b}$$
$$F_2^{n+1} = \sum_{m=0}^{3}\frac{e_m}{f_0}E^{n+1-m} - \sum_{m=1}^{2}\frac{f_m}{f_0}F_2^{n+1-m}, \tag{16c}$$

which are then fed back into (11) for the final update equation of the electric field E. Note that in 3D problems, a special treatment is required at the interfaces between DS and dielectric materials on the x-y plane, whose update equations are also obtained from the integral form of Maxwell's equations by proper volume averaging the values of media parameters.

The algorithm's validity is demonstrated by calculating the transmittance $T(f)$ of a 100-nm film of PEDOT:PSS, whose DS parameters are given in Table 1 [7]. The substrate is a 545-µm slice of lossless silica ($\varepsilon_s = 3.842$). Figure 2 shows the FDTD results compared to the analytical solution given by

$$t_{0123} = \frac{t_{01}t_{123}P_1}{1 - r_{10}r_{123}P_1^2}, \tag{17}$$

where $t_{ij} = 2n_i/(n_i + n_j)$ and $r_{ij} = (n_j - n_i)/(n_i + n_j)$ are the Fresnel transmittance and reflectance coefficients, respectively, at the interface between media i and j and $n_{i,j}$ their complex refractive indices. The rest of the parameters in (17) are $t_{123} = t_{12}t_{23}P_2/(1 - r_{21}r_{23}P_2^2)$, $r_{123} = (r_{12} + r_{23}P_2^2)/(1 + r_{12}r_{23}P_2^2)$, where $P_i = \exp(ikn_id_i)$, d_i being the thickness of medium i and k the free-space wavenumber. The FDTD spatial step $\Delta z = 1$ µm, i.e., one order of magnitude larger than the film thickness. The maximum error of the FDTD results in the examined spectrum is less than 0.7%. The oscillations in $T(f)$ stem from the Fabry-Pérot effect in the substrate. The spectra for $c = 0$ (Drude) and $c = -1$ (full backscattering) are also included, in order to demonstrate the algorithm's capability of modelling the full range of DS media.

Next, we experimentally study a thin layer of PEDOT:PSS (Clevios™ P Jet 700 conducting sulfonate polymer by Heraeus), having a nominal DC conductivity $\sigma_{\mathrm{DC}} = 667$ S/cm. The substrate is a 100-µm film of the cyclo-olefin polymer Zeonor (ZF14-100), an excellent substrate for THz components thanks to its record-low absorption losses, mechanical flexibility, and heat resistance [18]–[20]. First, the Zeonor substrate was treated with reactive ion-etching (O_2 ions for 90 sec) to promote adhesion of PEDOT:PSS on the hydrophobic substrate. Then, the PEDOT:PSS solution was spin-coated at 500 rpm for 60 sec for a nominal thickness of 50 nm. Finally, the sample was baked at 120°C for 15 min.

The sample was placed in the free-space beam path of a home-built THz-TDS setup, based on a mechanically tunable delay line as in Fig. 1(b). The setup employed a linearly-polarized fs-pulse laser at 800 nm and InGaAs photoconductive antennas with a peak response at 0.5 THz and a signal-to-noise ratio SNR> 40 dB. The measurements were performed in N_2 environment at a relative humidity of 0.1% at 22.5°C. A fast Fourier transform of the time-domain measured signal was employed to calculate the spectral characteristics of the transmitted THz wave transmitted. The total time scan was 100 ps, corresponding to a spectral resolution of 10 GHz.

The experimentally measured values were then fitted in the 0.3-1 THz window to the DS model using the nonlinear optimization Nelder-Mead technique implemented in the `fminsearch` function of Matlab™. The free variables were the DS parameters $\varepsilon_{DS,\infty}, \omega_p, \gamma$ and c, plus the film thickness t, which was constrained in a ±10% interval around 50 nm to account for small inaccuracies in the process of spin-coating. The minimized objective function was defined as

$$F = \sum_{i=1}^{N}\left|\frac{T_{m,i} - T_{c,i}}{T_{m,i}}\right| + \left|\frac{P_{m,i} - P_{c,i}}{P_{m,i}}\right|, \tag{18}$$

where the subscripts m and c refer to the TDS measured values of $T(f)$ and the accumulated phase $P(f)$ and those calculated via the analytical solution at each iteration of the optimization process. The sum runs for $N = 72$ values in the

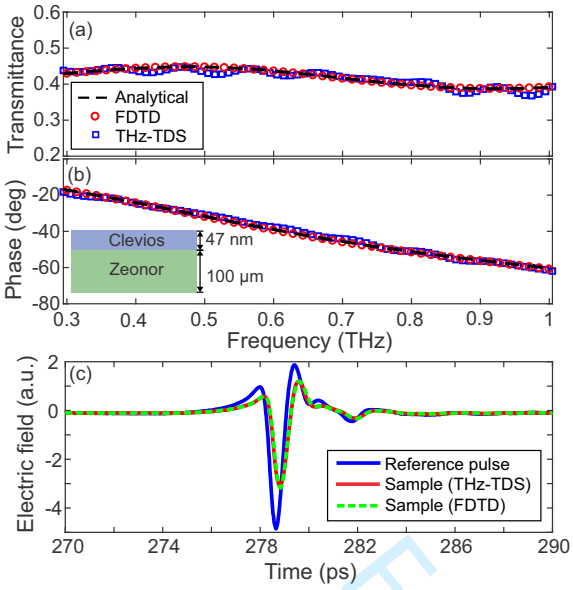

Fig. 3. (a) Transmittance and (b) accumulated phase of a 47-nm PEDOT:PSS (Clevios P Jet 700) layer on top of a Zeonor substrate measured via THz-TDS, fitted to the DS model and simulated by the proposed FDTD method. (c) Reference and sample THz signals.

0.3-1 THz window ($\Delta f = 10$ GHz), in which the SNR was greater than 20 dB. The fitting parameters are given in Table 1 for a derived thickness of $t = 47$ nm. The resulting DC conductivity $\sigma_{0,\mathrm{DC}} = (1 + c)\varepsilon_0\omega_p^2/\gamma$, is 663 S/cm, i.e., very close to the manufacturer's nominal value $\sigma_0 = 667$ S/cm.

Figure 3 provides a comparison of the sample characterization by means of THz-TDS, the FDTD algorithm ($\Delta z = 0.5$ μm), and the analytical solution. In the FDTD calculations, Zeonor was modeled as a Debye medium ($\varepsilon_{D,\infty} = 2.322$, $\varepsilon_{D,s} = 2.329$, and $\tau = 0.29$ ps), describing the very low dispersion of the material around the refractive index $n_Z = 1.525 - j0.001$ [21], [22]. Given that Zeonor's dielectric properties are well-known, its Debye parameters were not included in the fitting algorithm in order to avoid convergence issues and/or spurious solutions due to the increased number of unknowns. To reproduce the exact conditions of the experiment, the TDS-measured reference pulse was fed as excitation in the FDTD algorithm. Excellent agreement between the analytical and numerical results is observed. The slight rippling of the TDS measured values is not of physical origin and it is attributed to measurement noise. To compare with, the algorithm ran almost 2500 times faster and showed better overall performance than a DS-FDTD simulation without the subcell formulation and a uniform step of $\Delta z = 10$ nm.

III. Conclusions

In brief, we provide a complete characterization of PEDOT:PSS conducting films for THz applications based on the DS model, which captures correctly their EM properties. The analysis is backed by a subcell-based FDTD algorithm, capable of describing the dispersive nature of both the TCF and the dielectric substrate. The proposed methodology can be directly applied to the design of THz optoelectronic devices employing TCF as transparent electrodes.

References

[1] S. S. Dhillon *et al.*, "The 2017 terahertz science and technology roadmap," *J. Phys. D*, vol. 50, art. no. 043001, 2017.
[2] C.-S. Yang, T.-T. Tang, P.-H. Chen, R.-P. Pan, P. Yu, and C.-L. Pan, "Voltage-controlled liquid-crystal terahertz phase shifter with indium–tin–oxide nanowhiskers as transparent electrodes," *Opt. Lett.*, vol. 39, pp. 2511–2513, 2014.
[3] B. Vasić, D. C. Zografopoulos, G. Isić, R. Beccherelli, and R. Gajić, "Electrically tunable terahertz polarization converter based on overcoupled metal-isolator-metal metamaterials infiltrated with liquid crystals," *Nanotechnol.*, vol. 28, art. no. 124002, 2017.
[4] F. Yan, E. P. J. Parrott, B. S.-Y. Ung, and E. Pickwell-MacPherson, "Solvent doping of PEDOT/PSS: Effect on terahertz optoelectronic properties and utilization in terahertz devices," *J. Phys. Chem. C*, vol. 119, pp. 6813–6818, 2015.
[5] N. V. Smith, "Classical generalization of the Drude formula for the optical conductivity," *Phys. Rev. B*, vol. 64, art. no. 155106, 2001.
[6] G. Hwang, S. Balci, M. Z. Güngördü, A. Maleski, J. Waters, S. Lee, S. Choi, K. Kim, S. Cho, and S. M. Kim, "Flexibility and non-destructive conductivity measurements of ag nanowire based transparent conductive films via terahertz time domain spectroscopy," *Opt. Express*, vol. 25, pp. 4500–4508, 2017.
[7] T. Sasaki, H. Okuyama, M. Sakamoto, K. Noda, H. Okamoto, N. Kawatsuki, and H. Ono, "Twisted nematic liquid crystal cells with rubbed poly(3,4-ethylenedioxythiophene)/poly(styrenesulfonate) films for active polarization control of terahertz waves," *J. Appl. Phys.*, vol. 121, art. no. 143106, 2017.
[8] J. B. Baxter and C. A. Schmuttenmaer, "Conductivity of ZnO nanowires, nanoparticles, and thin films using time-resolved terahertz spectroscopy," *J. Phys. Chem. B*, vol. 110, pp. 25 229–25 239, 2006.
[9] H. J. Joyce, J. L. Boland, C. L. Davies, S. A. Baig, and M. B. Johnston, "A review of the electrical properties of semiconductor nanowires: insights gained from terahertz conductivity spectroscopy," *Semicond. Sci. Technol*, vol.. 31, art. no. 103003, 2016.
[10] C.-S. Yang, M.-H. Lin, C.-H. Chang, P. Yu, J.-M. Shieh, C.-H. Shen, O. Wada, and C.-L. Pan, "Non-drude behavior in indium-tin-oxide nanowhiskers and thin films investigated by transmission and reflection THz time-domain spectroscopy," *IEEE J. Quantum Electron.*, vol. 49, pp. 677–690, 2013.
[11] H. W. Liu, L. M. Wong, S. J. Wang, S. H. Tang, and X. H. Zhang, "Effect of oxygen stoichiometry on the insulator-metal phase transition in vanadium oxide thin films studied using optical pump-terahertz probe spectroscopy," *Appl. Phys. Lett.*, vol. 103, art. no. 151908, 2013.
[12] D. G. Cooke, A. N. MacDonald, A. Hryciw, J. Wang, Q. Li, A. Meldrum, and F. A. Hegmann, "Transient terahertz conductivity in photoexcited silicon nanocrystal films," *Phys. Rev. B*, vol. 73, art. no. 193311, 2006.
[13] R. Fastampa, L. Pilozzi, and M. Missori, "Cancellation of fabry-perot interference effects in terahertz time-domain spectroscopy of optically thin samples," *Phys. Rev. A*, vol. 95, art. no. 063831, 2017.
[14] A. Taflove and S. C. Hagness, *Computational Electrodynamics: The Finite-Difference Time-Domain Method.* Norwood, MA: 3rd ed., Artech House, 2005.
[15] D. C. Zografopoulos, K. P. Prokopidis, R. Dąbrowski, and R. Beccherelli, "Time-domain modeling of dispersive and lossy liquid-crystals for terahertz applications," *Opt. Mater. Express*, vol. 4, pp. 449–457, 2014.
[16] A. Mohammadi, T. Jalali, and M. Agio, "Dispersive contour-path algorithm for the two-dimensional finite-difference time-domain method," *Opt. Express*, vol. 16, pp. 7397–7406, 2008.
[17] K. Tekbas, F. Costen, J.-P. Berenger, R. Himeno, and H. Yokota, "Subcell modeling of frequency-dependent thin layers in the FDTD method," *IEEE Trans. Antennas Propag.*, vol. 65, pp. 278–286, 2017.
[18] A. Ferraro, D. C. Zografopoulos, M. Missori, M. Peccianti, R. Caputo, and R. Beccherelli, "Flexible terahertz wire grid polarizer with high extinction ratio and low loss," *Opt. Lett.*, vol. 41, pp. 2009–2012, 2016.
[19] A. Ferraro, D. C. Zografopoulos, R. Caputo, and R. Beccherelli, "Broad- and narrow-line terahertz filtering in frequency-selective surfaces patterned on thin low-loss polymer substrates," *IEEE J. Sel. Top. Quantum Electron.*, vol. 23, art. no. 8501308, 2017.
[20] ——, "Angle-resolved and polarization-dependent investigation of cross-shaped frequency-selective surface terahertz filters," *Appl. Phys. Lett.*, vol. 110, art. no. 141107, 2017.
[21] ——, "Terahertz polarizing component on cyclo-olefin polymer," *Photon. Lett. Pol.*, vol. 9, pp. 2–4, 2017.
[22] A. Podzorov and G. Gallot, "Low-loss polymers for terahertz applications," *Appl. Opt.*, vol. 47, pp. 3254–3257, 2008.